A Synchronous TDMA Ultrasonic TOF Measurement System for Low-Power Wireless Sensor Networks

Carlos Medina, José C. Segura, *Senior Member, IEEE*, and Ángel de la Torre

***Abstract*—This paper presents the design and evaluation of an ultrasonic time-of-flight (TOF) measurement system in the context of a smart sensor wireless network. In particular, the ZigBee protocol is used for data transmission and synchronization purposes. Low-cost and low-power restrictions are taken into account in the design. A synchronous measurement scheduling approach is used to minimize the network traffic and, therefore, the power consumption, while avoiding the need of wired connections between the nodes or the use of specific radio link to provide synchronization. A theoretical model that describes the accuracy of the proposed system is derived. This model takes into account both clock drift effects and finite clock resolution of the network nodes. According to the model, the estimation of the TOF is biased due to the clock drifts, and a solution is proposed to compensate this bias. The compensation is based on an accurate estimation that each node performs for its own clock drift. An error analysis of this estimation procedure is also developed, and its effects on the TOF accuracy are presented. A theoretical model of the system that predicts the system performance in terms of TOF accuracies is proposed. An implementation of the TOF measurement system is presented, from which experimental results that validate the theoretical derivations and the effect of the clock drift compensation are obtained. Experimental evaluation of the system also demonstrates that TOF accuracies better than 2 μs are achievable, which will be more than adequate for achieving subcentimetric or even submillimetric precisions in ultrasound-TOF-based distance measurement systems. Even though a particular approach for TOF estimation is considered in this work, most of the derived results are also applicable to other systems involving time synchronous measurements.**

***Index Terms*—Local positioning systems (LPSs), ultrasonic pseudorange measurement, wireless sensor networks.**

I. Introduction

THE USE of location information and its potential in the development of ambient intelligence applications has led in recent years the design and implementation of location systems. The main differences between local positioning systems (LPSs) are related to the type of technology used, conditioned by the requirements of infrastructure and system accuracy. Systems based on radio signals require fewer infrastructures than other technologies but offer lower precision: from tens of centimeters in ultrawideband systems using time-of-arrival measurements [1] to several meters for systems using the received-signal-strength-indicator measurements (Wi-Fi [2], ZigBee [3], and radio-frequency identification [4]). Advances in machine vision make achieving accuracies of several centimeters possible [5] at the cost of using an expensive infrastructure, low modularity, and high processing requirements.

An alternative solution is the use of ultrasonic signals. Unlike other technologies, ultrasound technology has certain advantages such as a slow signal propagation speed, no penetration of walls, lack of regulatory control, or low-cost transducers. This technology allows obtaining centimetric or even subcentimetric accuracies with a relatively low processing resource demand. In the literature, we find several examples of ultrasonic LPSs based on the measurement of the time of flight (TOF) of ultrasonic signals, the most representative being Active Bat [6], Cricket [7], Dolphin [8], and 3D-Locus [9], [10].

The time for the ultrasonic signal to travel the distance between a sending node and a receiving node is used for the estimation of the distance between these two nodes considering the sound propagation speed. Accurate TOF measurements require a proper synchronization of transmitter and receiver devices. In a wireless system architecture, the use of radio-frequency or infrared signals to provide such synchronization is common.

Recent developments on low-power smart sensor networks technology facilitate the implementation of low-cost low-energy ad hoc networks that can be used as the basic infrastructure for indoor location [11]. Therefore, adding ultrasonic TOF measurement capabilities to a smart sensor network opens the possibility to develop precise, low-cost, and versatile LPS or industrial positioning systems [9] with the advantage of removing the need of wired connections between ultrasonic sensors.

Several alternative solutions have been proposed for ultrasonic TOF measurement [12] with different levels of complexity and precision. For the present work, we have selected a TOF measurement technique based on a digital quadrature correlation receiver. A quadrature bandpass sampling [13], [14] scheme allows one to implement this technique with the limited memory and computational resources of the smart network nodes.

In this paper, we focus on the design and evaluation of an ultrasonic TOF measurement system to be used in a low-power

Manuscript received March 8, 2012; revised July 5, 2012; accepted August 7, 2012. Date of publication October 5, 2012; date of current version February 5, 2013. This work was supported in part by the Junta de Andalucía under Research Project P08-TIC-03886. The Associate Editor coordinating the review process for this paper was Dr. Serge Demidenko.

The authors are with the Department of Signal Theory, Telematics and Communications (TSTC) and the Information and Communications Technology Research Centre (CITIC), University of Granada (UGR), 18010 Granada, Spain (e-mail: cmedina@ugr.es; segura@ugr.es; atv@ugr.es).

Digital Object Identifier 10.1109/TIM.2012.2218056

wireless sensor network recently developed by the authors (TELIAMADE) [15], [16] based on the ZigBee network protocol [17].

TELIAMADE's nodes are built around a low-power microcontroller and an 802.15.4 wireless modem and interconnected through the ZigBee low-power network protocol. The restrictions of low cost and low power consumption (and therefore low network traffic) condition the design of the measurement system.

Both time division multiple access (TDMA) and code division multiple access (CDMA) techniques have been proposed in the context of ultrasonic TOF measurement systems. Using the first approach, each TOF measurement is scheduled at a different time to prevent signal overlapping. This is the case in [8]–[10], in which a master controller schedules each measurement by sending an appropriate synchronization signal (either using a wired connection or a specific radio link).

CDMA allows the simultaneous transmission of several ultrasonic signals [8]–[10]. Using BPSK modulation with an appropriate set of pseudorandom codes, each signal can be separated by correlation at the receiver. Even in this case, a synchronization signal is needed [9], [10] to be able to measure the TOF of each individual signal. Without this synchronization information, the receiver can only measure the TOF difference between different emitters' signals, provided that all of them have been emitted at the same time. Although the receiver can be operated asynchronously in this case, synchronization must be guaranteed among transmitters, which is implemented in [8] by sending a synchronization signal through a wired connection.

In both approaches, each TOF measurement needs a separate synchronization signal. In the proposed wireless architecture, this would involve the transmission of a ZigBee message to synchronize each measurement. This would generate high network traffic and, therefore, high power consumption of the wireless nodes.

TDMA is also used in [11] without the need of a specific synchronization signal for each measurement. Time instants of ultrasonic signal transmission and reception are scheduled based on timing provided by a TDMA temporal structure. In this approach, the need of a specific synchronization signal for every new measurement is removed. This avoids the need of wired connections or the use of a specific radio link. Due to these clear advantages, a similar TDMA scheduling approach is used in TELIAMADE but with higher synchronization accuracy. In addition, the impact of the synchronization accuracy in the achievable TOF accuracy is extensively discussed in this paper.

To illustrate the achievable network traffic reduction, consider the situation of performing five TOF measurements per second. Using one synchronization message per measurement will result in a five-messages-per-second traffic load. Using a TDMA scheduling approach, this value will only be dependent on the time interval between synchronization messages and not on the measurement rate. In the implementation described in this paper, we will show that an appropriate synchronization can be maintained with less than 0.3125 message per second, which represents a network traffic reduction by a factor of 16.

By using this approach, wired connections and specific radio links are avoided within a low complexity solution with low network traffic. The solution is implemented on standard ZigBee nodes with minor hardware and software modifications. Both theoretical and experimental results show that synchronization and TOF accuracies are similar or even better than those reported in [9] and [11].

Within this approach, management of all timing information in the system is based on the clock signal of the smart nodes. Although accurate crystal oscillators are used in the microcontroller of the nodes, different drifts in the nominal resonant frequency of the crystals entail synchronization errors affecting the measurements. Furthermore, the finite resolution of the clocks of the nodes introduces additional uncertainty. These potential error sources are studied in detail, and solutions are given to minimize the total TOF error.

Many synchronization protocols have been proposed in the context of wireless sensor networks with different accuracy levels. An extensive survey can be found in [18]. In this paper, we focus on protocols using the master–slave approach, in which the clocks of the nodes are synchronized with the clock of a special reference node (master node). Furthermore, we will also consider only those protocols designed for one-hop networks, in which all nodes in the network are accessible from any node in a single packet transmission. The main advantage is that a message transmitted by the master node is received at virtually the same time by all network nodes. Exploiting this fact, better synchronization accuracies can be obtained.

Most protocols are based on comparing the time stamps of message transmission and/or reception over the network. In the reference broadcast synchronization protocol [19], a set of receivers are synchronized with one another. A transmitter node sends a synchronization broadcast message, and the reception time is recorded by all receiver nodes according to its local clock. The receivers then exchange their observations, and based on this information, each receiver can compute the offset of its local clock with respect to each other. Considering a sequence of synchronization messages, each receiver can also compute the relative drift of its clock with respect to any other. The main drawback of this protocol is the high network traffic involved in the information exchange of reception time stamps and its high computational load.

To overcome this problem, alternative algorithms have been proposed in which the clocks of a set of slave nodes are synchronized to the clock of a master node. In this way, the need of information exchange between nodes is removed, and the computational complexity is reduced.

In continuous clock synchronization (CCS) [20], the master node sends a broadcast message which is received by all nodes (including the master node) at the same time. Each node time-stamps this message with its own clock. In a second message, the master node sends the time stamp obtained at the reception of the previously sent synchronization message. Using these time stamps, the nodes can estimate their clock offset. Using several consecutive synchronization messages, the nodes can also compute an estimation of its clock drift. The main limitation of this protocol is that the master node must be able to

receive the synchronization messages sent by itself, and this requires a major modification of the network protocol. Reported accuracies are on the order of 150 μs.

With the aim of avoiding the CCS limitations, at least two variants of the protocol have been proposed. In [21], the authors consider a linear relation between clocks that accounts for a time offset and a clock drift. Two consecutive synchronization messages are sent by the master node that are time-stamped by the master node and by the slave nodes. The differences between the time stamps are used by the slave nodes to perform an estimation of the offset and the drift of their clocks. The accuracy of this protocol is greatly dependent on the assumption of a constant delay between the time stamps of the transmission and reception of messages. By time-stamping the messages at the Medium Access Control (MAC) layer, the random variations are reduced, and accuracies on the order of ± 2 μs are reported. Another limitation of this protocol is the fact that only constant clock drifts are considered. Temporal variations of the clock drifts can degrade the performance, but this topic is not discussed in [21].

In [22], the authors propose a variant of CCS in which messages are also time-stamped at the MAC layer to minimize random variations between transmission and reception time stamps. Even doing that, the time differences between the transmission and reception of messages have a random behavior with a reported standard deviation of around 3.6 μs. As in [21], the differences between transmission and reception time stamps are used to estimate a linear model for each node that takes into account both a time offset and a clock drift for each node. Synchronization errors on the order of five clock periods are reported.

In this paper, we present a synchronization algorithm that is based on a similar approach to the ones used in [21] and [22]. The time differences between accurate time stamps of broadcast messages transmitted at the beginning of each multiframe of a TDMA temporal structure are used to compute a lineal model relating the clock of the end nodes to the clock of the master node. This allows the nodes to obtain a precise estimation of their own clock drift that is used to synchronize the emission and reception of ultrasonic signals. We provide a theoretical study of the effects of the resolution and drift of the clocks in terms of its impact on the accuracy of the TOF estimations. To the best of our knowledge, this is the first time that such an analysis is presented. From this analysis, we conclude that the contribution to the TOF standard deviation due to synchronization errors can be as low as 0.6 μs even with clock resolutions of 1 μs and clock drifts on the order of 50 parts per million (ppm). Experimental evaluation of the proposed measurement technique also demonstrates that TOF accuracies better than 2 μs are achievable even with inexpensive hardware within a wireless sensor network.

The rest of this paper is organized as follows. In Section II, the proposed synchronous TDMA measurement system is described. Section III is devoted to the timing issues in the proposed system. The effect of different clock drifts in TOF estimations is analyzed, showing that a bias in the TOF measurements appears as a result. A solution is presented to avoid this problem based on an estimation of the relative clock drift between nodes. Section IV discusses the proposed relative drift estimation algorithm along with a detailed error analysis. In Section V, a theoretical error analysis of the complete TOF measurement system is presented that takes into account both the clock drifts and the finite clock resolution of the smart nodes. A mathematical expression is derived for the effect of these error sources, from which a precision limit is obtained for the proposed system. Section VI shows the experimental results of the implemented measurement system which validate the theoretical derivations. Experimental results also demonstrate that, even with clock resolutions of 1 μs and clock drifts on the order of 50 ppm, subcentimetric pseudorange precisions can be easily achieved with the proposed system at distances of 2–5.5 m. Finally, Section VII summarizes the conclusions of this work.

II. Measurement System Description

The TELIAMADE system is based on a wireless network of smart nodes. Network architecture is based on the ZigBee protocol which fits the low power requirements for the smart sensor network design. A star network topology is used with a network coordinator and a set of end nodes. End nodes are equipped with a low-power microcontroller (PIC18F4620) [23] and a radio chip (CC2420) [24] implementing the 802.15.4 physical layer. The rest of the ZigBee stack is implemented by software in the microcontroller.

Each TELIAMADE node is also equipped with a couple of low-cost ceramic ultrasonic transducers (400ST/R120) [25] with a center frequency of 40 kHz and a 6-dB bandwidth of 2 kHz. Therefore, a given node can be configured to transmit or receive an ultrasonic signal at a given time. TOF estimations are obtained by measuring the propagation delay of a 1-ms ultrasonic signal between a couple of nodes, one acting as an ultrasonic emitter and the other as an ultrasonic receiver. The ultrasonic receiver node also performs the TOF estimation.

Generation of an ultrasonic burst is performed by the Enhanced Universal Synchronous Asynchronous Receiver Transmitter (EUSART) of the microcontroller. A sequence of alternating 0 and 1 b is generated at a baud rate of twice the nominal frequency of the transducer (i.e., 80 kb/s) with an appropriate length (i.e., a 1-ms burst requires the transmission of a sequence of 80 alternating bits). The EUSART output is buffered though a digital inverter gate (74HC04) [26] to provide the needed current gain to drive the ultrasonic transducer.

Computation of the TOF is performed by the receiver node using a quadrature digital correlator. The signal from the ultrasonic transducer is amplified and filtered using a second-order analog active filter with a center frequency of 40 kHz and a quality factor $Q = 8$. This preamplification and filtering stage is implemented with a dual operational amplifier chip (LMC6482) [27]. The conditioned signal is then sampled and stored in a memory buffer. A bandpass sampling scheme [13], [14] is used to reduce the required memory and processing resources. In this way, the computation of the TOF can be autonomously performed by the receptor node. The digital receiver is operated at a sampling frequency of 17.78 kHz, which allows

managing single-sided reception bandwidths of 4.45 kHz. A buffer size of 1067 B is used to store the samples (assuming 2-B samples and a maximum TOF of 30 ms). In-phase and quadrature components are obtained from the sampled data, and two correlators are used to obtain the in-phase and quadrature outputs. Finally, the envelope at the correlator output is obtained from these two components. The position of the maximum value of the correlator output is used as the first estimation of the TOF. Parabolic interpolation [28] around the position of this maximum is then used to obtain a time resolution much better than one-half sample. Finally, an estimation of the TOF is obtained as an integer number of samples (position of the maximum) plus a fractional number of samples (output of the parabolic interpolation) and then converted to time units using the nominal value of the sampling frequency.

The overall complexity and cost of the additional hardware are very low in comparison with those of the standard ZigBee hardware. It only consists of a couple of ultrasonic transducers, one operational amplifier chip, one digital inverter buffer, and several resistors and capacitors. The average consumption of the ZigBee module is 25 mA, and the additional hardware consumption is 5 mA, which leads to a total amount of 30 mA in normal operation. When the system is put in sleep mode, the consumption is reduced to 1.7 mA. Therefore, when powered with a typical 2000-mA battery, a node can be operated during 67 and 1176 h in normal measurement mode and in sleep mode, respectively. The consumption is further reduced with the use of the synchronous TDMA measurement scheduling presented in the next section.

A. TDMA Synchronization

In order to obtain an accurate estimation of the TOF, the receiver needs to know the time instant when the transmitter starts the generation of the ultrasonic pulse. A possible solution is to use a ZigBee message to fire the TOF measurement process simultaneously in both the transmitter and the receiver. In this way, the receiver can estimate the TOF as the time delay between the start of the reception and the time that the ultrasonic pulse is detected. Although this scheme guarantees adequate time synchronization and therefore corrects TOF estimates, it has some disadvantages. First, it requires that all network nodes remain actively listening to the radio interface. This prevents the nodes to be in sleep mode with the consequent increase in power consumption. Second, this scheme involves high network traffic, particularly considering situations with high measurement rate.

A more efficient solution is to use a periodic prescheduled measurement scheme based on a TDMA approach. This is a common approach in digital communication systems to provide time synchronization [29]. Using this approach, the network nodes can be programmed to start transmission or reception of ultrasonic pulses at given time instants. These time instants can be fixed using a temporal structure like the one shown in Fig. 1.

In this example, the TDMA structure is organized in periods of 6.4 s, which we will refer to as a multiframe. The beginning of each multiframe is signaled by the network coordinator by sending a synchronization message (Msync) which all network nodes receive at the same time (neglecting the propagation delay of the radio signal[1]). Each multiframe is divided into 32 frames of 200 ms, and the beginning of each frame is used as the time instant to begin a TOF measurement process. Using this scheme, the network traffic due to synchronization is now independent of the measurement rate, and it is only conditioned by the information needed to maintain a proper synchronization. As we will show later in Section IV, two messages per multiframe are enough to maintain synchronization. Therefore, the network traffic due to synchronization is reduced to two messages per multiframe, which corresponds to a reduction in a factor of 16.

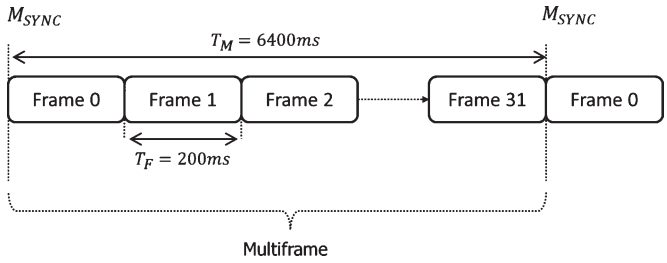

Fig. 1. TDMA temporal structure used for measurement scheduling.

An additional advantage of using this measurement scheduling approach is a reduction in the average consumption of the nodes. Without the need of sending a specific synchronization message for every new measurement, the end nodes put its radio chip in an idle state most of the time and only activate it to receive the synchronization message at the beginning of every new multiframe. The averaged consumption of an end node with the radio chip in receive state is around 30 mA, while the consumption of the radio chip alone is 18.8 mA. By maintaining the radio chip in an idle state during all but the first frame of the multiframe, the averaged consumption of the nodes is reduced to 11.8 mA. This will enlarge the life of the batteries in a factor of 2.5. When powered with a 2000-mA battery, the nodes can operate in measurement mode for around 167 h.

In order to find the beginning of a given frame in the multiframe, each network node maintains a local tick counter that is reset at the beginning of each multiframe (upon the reception of the synchronization message). At any given time instant, each node can compute the frame number as follows. Consider Δt as the time offset from the reception of the synchronization message at the beginning of the multiframe. Then, the frame number is computed as

$$n_F = \left\lfloor \frac{\Delta t}{T_F} \right\rfloor \tag{1}$$

where T_F is the frame duration. The time offset from the beginning of the current frame is

$$\Delta t_o = \Delta t - n_F T_F. \tag{2}$$

[1]For typical ultrasound distance measurements of less than 10 m, the propagation delay of a radio signal is on the order of 0.033 μs. The distance error due to this delay (for a typical sound speed of 340 m/s) would be only 0.011 mm, at least one order of magnitude inferior to other error sources considered in this work.

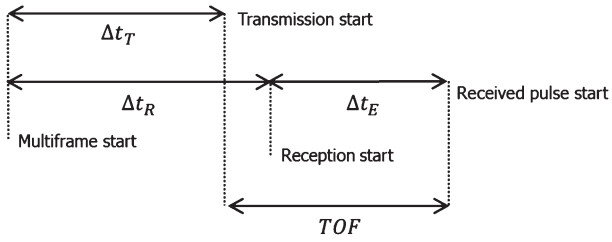

Fig. 2. Schematic timing diagram of TOF measurement.

In a general scenario, each transmitter node starts the ultrasonic pulse generation at the beginning of a predefined frame of the multiframe. The receptor node starts the reception process of the ultrasonic pulse at the beginning of this same frame, which guarantees that both processes start at the same time. The time elapsed since the beginning of the reception process until the pulse is detected is therefore the TOF of the ultrasonic signal, from which the distance can be obtained using the sound speed. The frame duration in this example ($T_F = 200$ ms) is selected to allow a maximum of five pseudorange measurements per second. The number of frames is selected to allocate a maximum of 32 transmitter nodes (each one assigned to a different frame of the multiframe). Changing the number of frames and the frame duration, the TDMA structure can be configured to fit other measurement scenarios.

III. Timing Issues

Timing information in the network nodes is derived from the clocks of their microcontrollers, which are, in turn, driven by crystal oscillators. Variations on the order of several tens of parts per million of the nominal resonant frequency are common for commercial crystals. As a result, all time measurements made with a microcontroller clock are affected by a drift. Different clock drifts for each node result in synchronization errors that degrade the system performance by adding an unknown bias to the TOF estimations.

In this section, a timing analysis of the TOF measurement process is presented, and the effect of clock drifts is analyzed. A different clock drift β_n is assumed for each node to account for the relative variation of the crystal oscillator nominal period.[2] The relation between a time interval Δt and the corresponding value $(\Delta t)_n$ measured by a node with a clock drift β_n is

$$\Delta t = (1 + \beta_n)(\Delta t)_n. \tag{3}$$

In the following, the subindex n is used to refer to a given node (either an ultrasonic transmitter or receiver node). It can be replaced by T when referring to a transmitter node and by R for a receiver node.

Fig. 2 shows a schematic diagram of times involved in the TOF computation between a transmitter (T) node and a receiver (R) node. Δt_T is the time elapsed between the start of the multiframe and the start of the ultrasonic pulse generation by the transmitter node. Similarly, Δt_R is the time elapsed between the start of the multiframe and the start of the sampling process in the receiver node, and Δt_E is the delay of the ultrasonic pulse from the beginning of the sampling process. The TOF can be written down in terms of these values as

$$\Delta t_E = \mathrm{TOF} + (\Delta t_T - \Delta t_R). \tag{4}$$

In the following, we will analyze the effect of clock drifts, assuming for the moment that the clocks have an infinite resolution. Consider the case of a TOF measurement scheduled at frame n_F of the multiframe. Each node n (transmitter or receiver) implements the nominal delay $n_F T_F$ (from the multiframe start to the beginning of the frame n_F), but due to its clock drift, the actual value of the delay will be

$$\Delta t_n = n_F T_F (1 + \beta_n). \tag{5}$$

As both transmitter and receiver proceed in the same way, the following relations can be written for the Δt_T and Δt_R delays

$$\Delta t_T = n_F T_F (1 + \beta_T) \tag{6}$$

$$\Delta t_R = n_F T_F (1 + \beta_R) \tag{7}$$

where β_T and β_R are the drifts of the transmitter and receiver clocks, respectively. Using (4), (6), and (7), we can write down a new relation between Δt_E and TOF as

$$\Delta t_E = \mathrm{TOF} + n_F T_F (\beta_T - \beta_R) \tag{8}$$

from which it is evident that Δt_E is a biased estimate of the TOF. The bias is a function of the difference between the clock drifts, the frame number, and the frame duration. The maximum bias error occurs at the last frame $n_F = 31$. For $T_F = 200$ ms and clock drifts on the order of 50 ppm, this bias can be as large as 620 μs (or 21 cm for a typical sound speed of 340 m/s). Direct compensation of this bias requires the receiver node to precisely know its own clock drift β_R and also the transmitter node clock drift β_T. This needs a calibration process with a precise reference clock. A simpler solution is presented in the following section, which also allows one to track temporal variations of the clock drifts (for example, those due to thermal variations).

A. Avoiding the Bias Due to Different Clock Drifts

The bias term can be avoided if all network nodes share a common time base provided by the network coordinator. To this end, each network node performs an estimation of the common time (the coordinator time) using a linear transformation of its local time.

The relation between the measurement of a time interval Δt with the coordinator clock $(\Delta t)_c$ and with a network node clock $(\Delta t)_n$ is

$$(\Delta t)_c = (1 + \alpha_n)(\Delta t)_n \tag{9}$$

where α_n is the clock drift of the node n relative to the coordinator clock and is related to the clock drifts of the coordinator

[2]Note that, contrary to what is common, in this paper, we define the drift as a relative period variation rather than as a relative frequency variation.

β_c and the node β_n by

$$1+\alpha_n = \frac{1+\beta_n}{1+\beta_c}. \tag{10}$$

By using (9), each node can transform (given that α_n is known) a time interval measured with the coordinator clock into units of its own clock and vice versa.

Consider again the case of a TOF measurement scheduled at frame n_F of the multiframe. Each node assumes that this value is expressed in units of the coordinator clock and transforms it using (9) into its own clock units, yielding a value of $\widetilde{n_F T_F} = n_F T_F/(1+\alpha_n)$. Due to the clock drift β_n of the node, the implemented delay will be

$$\begin{aligned}\widetilde{\Delta t_n} &= \widetilde{n_F T_F}(1+\beta_n)\\ &= \frac{n_F T_F(1+\beta_n)}{(1+\alpha_n)}\\ &= n_F T_F(1+\beta_c) = \Delta t_c.\end{aligned} \tag{11}$$

This is nothing but the delay that the coordinator would have waited. Note that this is a fixed value, independent of the considered node. This way, both the transmitter and receiver nodes implement the same delay, and therefore, the bias in (8) is removed.

IV. Estimation of α

To implement the previously described algorithm, each network node must estimate its α value. This can be done by using synchronization information sent by the network coordinator at the beginning of each multiframe. In this section, we present the complete α estimation algorithm along with a detailed error analysis that takes into account the finite clock resolution.

Let us define the α estimator for a given network node as follows:

$$\begin{aligned}\tilde{\alpha}_n(k) &= \frac{\Delta N_c(k) T_c}{\Delta N_n(k) T_o} - 1\\ &= \frac{(N_c(k) - N_c(k-1))\, T_c}{(N_n(k) - N_n(k-1))\, T_o} - 1\end{aligned} \tag{12}$$

where $N_c(k)$ and $N_n(k)$ are the numbers of coordinator and node clock ticks at the arrival of the synchronization message signaling the beginning of multiframe k and $N_c(k-1)$ and $N_n(k-1)$ are the corresponding values at multiframe $k-1$. T_c and T_o are the coordinator and node clock nominal resolutions, respectively.[3] As we will show later, this is an unbiased estimator of α_n.

Obtaining the tick count $N_n(k)$ is easy. It only requires retrieving the local clock tick count at the reception of the synchronization message. Obtaining the corresponding tick count of the coordinator $N_c(k)$ is more difficult because it corresponds to the coordinator's tick count at the time that the synchronization message was sent. In our current implementation of the protocol, two consecutive messages are sent by the coordinator at the beginning of each multiframe.

From the first message, only the reception tick count $N_n(k)$ is used (which is obtained from the node clock). In the second message payload, the coordinator sends the tick count $N_c(k)$ corresponding to the time instant that the previous message was sent (these are ticks of the coordinator clock). Therefore, $N_n(k)$ and $N_c(k)$ are tick counts corresponding to a common time instant but obtained from the node and coordinator clocks, respectively. In this way, each network node can retrieve the needed information to estimate its own α.

To implement this algorithm, a minor modification of the MAC layer is needed to record the clock tick values just at the beginning of the reception of a radio packet and just at the end of the transmission of a radio packet. In our implementation, the MAC layer code of the ZigBee protocol stack is modified to record these tick counts.

A. Mean and Standard Deviation of the Estimator

The time at which the multiframe k synchronization message arrives at the node can be expressed as

$$t_s(k) = (N_n(k) + \varepsilon_n(k))\,(1+\beta_n) T_o \tag{13}$$

where $N_n(k)$ is an integer number of clock ticks of a given node n at the arrival of the synchronization message k and $\varepsilon_n(k)$ is an uncorrelated random process uniformly distributed in [0, 1] that takes into account the quantization effects due to the finite clock resolution T_o of the node.

The time interval between the arrival of two consecutive synchronization messages at multiframes $k-1$ and k will be

$$\begin{aligned}\Delta t_s(k) &= (t_s(k) - t_s(k-1))\\ &= (\Delta N_n(k) + \Delta\varepsilon_n(k))\,(1+\beta_n) T_o.\end{aligned} \tag{14}$$

A similar expression can be used for the same time interval measured with the coordinator clock

$$\Delta t_s(k) = (\Delta N_c(k) + \Delta\varepsilon_c(k))\,(1+\beta_c) T_c \tag{15}$$

where T_c is the nominal coordinator clock resolution. By equating (14) and (15) and using the definition (12), we can write down the following expression for the estimator:

$$\tilde{\alpha}_n(k) = \alpha_n + \frac{\Delta\varepsilon_n(k)(1+\alpha_n) - \Delta\varepsilon_c(k)\left(\frac{T_c}{T_o}\right)}{\Delta N_n(k)}. \tag{16}$$

Since $\varepsilon_n(k)$ and $\varepsilon_c(k)$ are uncorrelated uniformly distributed random processes in [0, 1], $\Delta\varepsilon_n(k)$ and $\Delta\varepsilon_c(k)$ will be the difference of two uncorrelated uniformly distributed random processes. We can obtain the expected value and variance of the estimator as follows:

$$E\left[\tilde{\alpha}_n(k)\right] = \alpha_n \tag{17}$$

$$\mathrm{Var}\left[\tilde{\alpha}_n(k)\right] = \frac{(1+\alpha_n)^2 + \left(\frac{T_c}{T_o}\right)^2}{6\left(\Delta N_n(k)\right)^2} \tag{18}$$

[3] We use T_o instead of T_n to designate the nominal clock resolution of the nodes to emphasize the fact that this resolution is considered equal for all nodes either acting as transmitter or receiver of ultrasonic signals.

TABLE I
THEORETICAL AND SIMULATED STANDARD DEVIATIONS σ OF α ESTIMATIONS FOR DIFFERENT COORDINATOR (T_c) AND NODE (T_o) CLOCK RESOLUTIONS. THEORETICAL VALUES (THEO) ARE OBTAINED WITH (18). MONTE CARLO SIMULATED VALUES (SIM) ARE SHOWN FOR TWO DIFFERENT VALUES OF THE IIR FILTER COEFFICIENT a. AVERAGED MEAN VALUES ARE EQUAL TO 50.0013 ppm IN ALL CASES

		Theo	Sim a=1.0	Sim a=0.2	Sim a=0.1
Tc (μs)	To (μs)	σ (ppm)	σ (ppm)	σ (ppm)	σ (ppm)
1	1	0.0902	0.0902	0.0134	0.0065
2	1	0.1426	0.1426	0.0213	0.0104
2	2	0.1804	0.1807	0.0269	0.0131

where $\Delta N_n(k)$ is the number of node clock ticks between two consecutive synchronization messages that can be approximated as

$$\Delta N_n(k) = \left\lfloor \frac{T_M}{T_o} \right\rfloor \tag{19}$$

assuming that the mean time between consecutive synchronization messages is equal to the multiframe duration (T_M).

The variance (18) can have a significant contribution to the total variance of the TOF estimation, as we will show later. For example, for $T_c = 2$ μs, $T_o = 1$ μs, $\alpha_n = 50$ ppm, and $n_F T_F = 6.4$ s, the square root of (18) will be 0.1426 ppm. A variance reduction can be obtained by averaging the consecutive estimations.

The network nodes compute their $\tilde{\alpha}_n(k)$ estimate every new multiframe k, and this information can be used to obtain a better estimation with a lower variance. For a constant or slow varying random process, a simple first-order IIR filter can be used to track the mean value

$$\hat{\alpha}_n(k) = a\tilde{\alpha}_n(k) + (1-a)\hat{\alpha}_n(k-1) \tag{20}$$

where the optimal a can be estimated based on the autocorrelation of $\tilde{\alpha}_n(k)$ or can be experimentally adjusted.

Monte Carlo simulations have been conducted to validate the aforementioned results. The time interval between synchronization messages was simulated as a Gaussian random variable with a mean of 6.4 s (the multiframe duration) and a standard deviation of 0.25 ms (to simulate a coordinator random delay in sending the synchronization messages). The relative coordinator and node clock drifts were fixed at $\beta_c = -25$ ppm and $\beta_n = 25$ ppm, respectively, corresponding to an α_n value of around 50 ppm. A total number of 200 simulations of 10^6 multiframe synchronization messages were performed for different coordinator and node clock resolutions. Averaged results are shown in Table I for different values of the IIR filter coefficient a. The mean values in all cases are equal to the theoretical value of 50.0013 ppm given by (10) for $\beta_c = -25$ ppm and $\beta_n = 25$ ppm. The standard deviations in the case of $a = 1.0$ also agree with the theoretical values given by (18) (when no IIR filtering is used). Finally, for the case of using an IIR filter with $a = 0.2$, the simulation predicts a reduction of the standard deviation in a factor of around 6.7 and in a factor of 13.7 for $a = 0.1$.

V. ERROR ANALYSIS OF TOF ESTIMATION

In this section, a complete error analysis of the TOF measurement system is presented. Clock drifts and finite clock resolution are taken into account in the derivation. We consider that each node n implements the α estimation algorithm described in the previous section and that an estimated value

$$\hat{\alpha}_n = \alpha_n + \xi_n \tag{21}$$

is available at the current multiframe (reference to the multiframe index k is removed in the following to simplify the notation) with ξ_n as a zero mean error term with standard deviation given in Table I.

Consider again the case of a TOF measurement scheduled at frame n_F of the multiframe. Each node n implements a delay of $n_F T_F/(1+\hat{\alpha}_n)$ seconds (in its own clock units) from the multiframe start before starting the transmission or reception process (depending on its configuration) by counting the corresponding number of ticks M_n given by

$$M_n = \left\lfloor \frac{n_F T_F}{(1+\hat{\alpha}_n)T_o} \right\rfloor = \frac{n_F T_F}{(1+\hat{\alpha}_n)T_o} - \upsilon_n \tag{22}$$

where υ_n is considered a random variable uniformly distributed in [0, 1] and independent of ε_n. Therefore, the time at which the node starts, the generation or reception of an ultrasonic pulse is

$$t_n = (N_n + M_n)(1+\beta_n)T_o. \tag{23}$$

This leads to a delay (using (13) for the current multiframe start)

$$\widehat{\Delta t_n} = t_n - t_s = n_F T_F \frac{1+\beta_n}{1+\hat{\alpha}_n} - (\varepsilon_n + \upsilon_n)(1+\beta_n)T_o. \tag{24}$$

To simplify the error analysis due to the variance of $\hat{\alpha}_n$, we perform the approximation

$$\frac{1}{1+\hat{\alpha}_n} = \frac{1}{1+\alpha_n+\xi_n} \simeq \frac{1}{1+\alpha_n} - \frac{\xi_n}{(1+\alpha_n)^2}. \tag{25}$$

Using (24), (25), and (10), we can derive the following expression for the delay:

$$\widehat{\Delta t_n} = n_F T_F(1+\beta_c) - n_F T_F \frac{1+\beta_c}{1+\alpha_n}\xi_n - (\varepsilon_n + \upsilon_n)(1+\beta_n)T_o. \tag{26}$$

Using (26) for both $\widehat{\Delta t_T}$ and $\widehat{\Delta t_R}$, the time difference (4) is now given by

$$\widehat{\Delta t_E} = \mathrm{TOF} + \left(\frac{\xi_R}{1+\alpha_R} - \frac{\xi_T}{1+\alpha_T}\right)(1+\beta_c)n_F T_F + \left((\varepsilon_R+\upsilon_R)(1+\beta_R) - (\varepsilon_T+\upsilon_T)(1+\beta_T)\right)T_o. \tag{27}$$

A. Other Error Sources

Estimation of Δt_E is performed by the receptor node using a digital correlator, and the delay is obtained in units of samples of the ultrasonic signal. The estimation can be modeled as

$$\overline{\Delta t_E} = \widehat{\Delta t_E} + b + \eta \tag{28}$$

where b is a bias term due to the group delay of the transducers and the analog bandpass filter and η is a zero mean random term which depends on the SNR of the received ultrasonic signal.

For a nominal sampling period T_s, the actual sampling period of the receptor node is $\widetilde{T_s} = T_s(1+\beta_R)$. The measured delay in units of samples will be

$$N_s = \frac{\overline{\Delta t_E}}{T_s(1+\beta_R)}. \tag{29}$$

Moreover, the estimated delay (obtained using the nominal sampling period) will be

$$\widetilde{\Delta t_E} = N_s T_s = \frac{\overline{\Delta t_E}}{(1+\beta_R)}. \tag{30}$$

Although $\widetilde{\Delta t_E}$ and $\overline{\Delta t_E}$ are related by $(1+\beta_R)$, the latter value is unknown to the receiver, and therefore, its TOF estimation can be based only on $\widetilde{\Delta t_E}$. For this reason, we choose to perform the error analysis in this variable.

By using (30), (28), and (27), we can finally write down the following expression for the TOF estimation:

$$\begin{aligned}\widetilde{\Delta t_E} = {} & \mathrm{TOF} + b - \frac{\beta_R}{1+\beta_R}(\mathrm{TOF}+b) + \frac{\eta}{1+\beta_R} \\ & + \frac{n_F T_F}{1+\alpha_R}\left(\frac{\xi_R}{1+\alpha_R} - \frac{\xi_T}{1+\alpha_T}\right) \\ & + T_o \frac{(\varepsilon_R+\upsilon_R)(1+\beta_R) - (\varepsilon_T+\upsilon_T)(1+\beta_T)}{1+\beta_R}. \end{aligned} \tag{31}$$

The expected value and variance of the estimator can be evaluated by considering that all random terms in (31) are independent

$$\begin{aligned} E[\widetilde{\Delta t_E}] = {} & \mathrm{TOF} + b - \frac{\beta_R}{1+\beta_R}(\mathrm{TOF}+b) \\ & + T_o \frac{\beta_R - \beta_T}{1+\beta_R} \end{aligned} \tag{32}$$

$$\begin{aligned} \mathrm{Var}[\widetilde{\Delta t_E}] = {} & \frac{\sigma_\eta^2}{(1+\beta_R)^2} \\ & + \left(n_F T_F \frac{1+\beta_c}{1+\beta_R}\right)^2 \left(\left(\frac{1+\beta_c}{1+\beta_R}\right)^2 + \left(\frac{1+\beta_c}{1+\beta_T}\right)^2\right)\sigma_\xi^2 \\ & + \frac{T_o^2}{6}\left(1 + \left(\frac{1+\beta_T}{1+\beta_R}\right)^2\right) \end{aligned} \tag{33}$$

where σ_ξ^2 is the variance in the estimation of α for both transmitter and receiver nodes. An approximation for the mean and variance can be obtained by letting $1+\beta_c \simeq 1+\beta_R \simeq 1+\beta_T \simeq 1$

$$E[\widetilde{\Delta t_E}] \simeq \mathrm{TOF} + b - \beta_R(\mathrm{TOF}+b) + T_o(\beta_R - \beta_T) \tag{34}$$

$$\mathrm{Var}[\widetilde{\Delta t_E}] \simeq \sigma_\eta^2 + \frac{T_o^2}{3} + 2(n_F T_F)^2 \sigma_\xi^2. \tag{35}$$

B. Estimated Order of Magnitude of the Different Errors

To show that the proposed approach can be accurate enough, we perform here an evaluation of the order of magnitude of errors affecting the TOF estimate using (34) and (35). The typical values considered for the parameters will be $T_o = 1$ μs for the clock resolution, $|\beta_T| \leq 50$ ppm and $|\beta_R| \leq 50$ ppm for the relative clock drifts, and TOF ≤ 30 ms (for a maximum pseudorange of around 10 m) and $b = 0.25$ ms for the group delay.

For the aforementioned values, the bias term $T_o(\beta_R - \beta_T)$ in (34) has a maximum value of 10^{-4} μs and can therefore be neglected. The term $\beta_R(TOF + b)$ is a TOF-dependent bias whose maximum values are 1.5 μs at 10 m and only 0.75 μs at 5 m. However, in any case, it can be partially removed along with the constant bias b by calibration.

The variance in (35) contains three terms. The first one corresponds to the variance of the correlator output estimate σ_η^2. The second term $T_o^2/3$ depends on the clock resolution. For a 1-μs resolution, the standard deviation will be 0.58 μs. The last term is the contribution of the variance in the estimation of α. Its value depends on the time offset $n_F T_F$ from the beginning of the multiframe. Therefore, TOF measurements will have a different variance depending on the frame at which the measurement is performed. The measurements performed in the first frame $(n_F = 0)$ will have no contribution of this term, while the measurements performed in the last frame $(n_F = 31)$ will have a significant contribution of this term. Considering a typical value of $\sigma_\xi = 0.1426$ ppm (see Table I without IIR filtering), the maximum rms contribution of this term will be 1.25 μs. When the IIR filtering is used with a value $a = 0.1$, a typical value of $\sigma_\xi = 0.0104$ ppm is obtained instead, and the maximum rms value of this term is reduced to 0.09 μs.

The joint contribution to the TOF rms error of the last two terms in (35) will be less than 0.6 μs or 0.2 mm at 340 m/s. This is the theoretical performance limit due to the finite clock resolution and the different clock drifts of the network nodes. Reducing the clock resolution T_o from 1 to 0.25 μs will reduce the corresponding rms contribution to 0.14 μs and the joint rms contribution to 0.17 μs or 0.06 mm at 340 m/s. For these values, the total TOF rms error will be almost independent of the clock drifts and resolution and more than adequate for subcentimeter precisions.

VI. Experimental Results

In this section, experimental results showing the effectiveness of the proposed synchronous measurement system are shown. The algorithms presented in this paper have been implemented in the TELIAMADE local positioning sensor network.

A. Experimental Setup

For the following experiments, one coordinator node (Nc) and six end nodes (numbered from N1 to N6) are used.

Several factors can cause additional TOF estimation errors; one of the most important is the multipath effect. The reflection of the ultrasonic signal in surrounding obstacles can create

alternative propagation paths between emitter and receiver. In some situations, the multipath effect can cause the overlapping of two or more replicas of the ultrasonic signals at the receiver, modifying therefore the shape of the received signal. This shape modification will introduce an unknown bias in the TOF estimation obtained by the receiver correlator. Dealing with such effects is not the purpose of this work, and therefore, we have used an experimental setup specifically designed to avoid them. When measuring the TOF between two network nodes, they are placed one in front of the other at a height of 1.6 m above the floor and 1.6 m farther away from walls and any other obstacle. For distances between emitter and receiver of less than 6 m, this setup ensures that any possible echo of the ultrasonic signal will reach the receiver at least 2.35 ms later than the main signal (the one propagated through the direct path). Considering that 1-ms ultrasonic signals are used in the experiments, this setup will avoid signal overlapping at the receiver due to multipath effects.

Unless otherwise stated, the system parameters were fixed as follows: number of frames $n_F = 32$, frame duration $T_F = 200$ ms, carrier frequency $F_c = 40$ kHz, sampling frequency $F_s = 17.78$ kHz, IIR filter coefficient $a = 0.1$, ultrasonic pulse duration of 1 ms, coordinator clock resolution $T_c = 2$ μs, and end-node clock resolution $T_o = 1$ μs.

B. Clock Drift Characterization

Clock drift characterization was based in measuring the frequency shift of the EUSART clock signal of each node. Due to the node clock drift, the nominal frequency F_b will result in an actual frequency

$$\widetilde{F_b} = F_b + \Delta F_b = \frac{F_b}{1+\beta_n}. \tag{36}$$

Therefore, the drift can be obtained as

$$\beta_n = -\frac{\Delta F_b}{F_b + \Delta F_b}. \tag{37}$$

For a nominal frequency of the EUSART clock $F_b = 80$ kHz and a clock drift value of $\beta_n = 50$ ppm, the value of the frequency shift will be $\Delta F_b = 4$ Hz. Measuring this small frequency deviation is difficult by directly analyzing the EUSART clock signal.

Instead of doing that, one can translate the signal to a lower frequency band by mixing it with a second signal of an appropriate frequency [30]. By multiplicative mixing the EUSART clock signal $\widetilde{F_b}$ with a reference signal of frequency $F_m = F_b + F_x/4$ and band-limiting the resulting signal to $F_x/2$, it is easy to show (although out of the scope of this paper) that the resulting signal will have only one frequency component at $F_d = F_x/4 - \Delta F_b$, provided that $|\Delta F_b| < F_x/4$.

If we select $F_x = 500$ Hz, the measurable range for the frequency shift ΔF_b will be ± 125 Hz. This will be adequate for estimating clock drifts up to several hundreds of parts per million. The frequency shift can be more precisely estimated because the frequency range of the new signal is centered on $F_x/4 = 125$ Hz instead on $F_b = 80$ kHz. The following procedure is used to obtain a precise estimation of the clock drift.

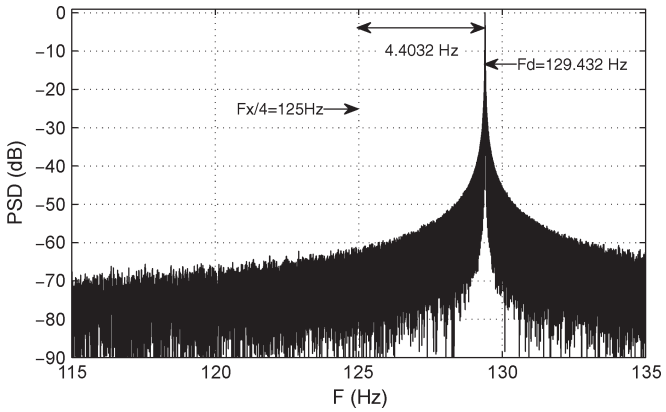

Fig. 3. Normalized Power Spectral Density of node N1 data showing a frequency shift of 4.4032 Hz corresponding to a relative drift of 55.04 ppm.

TABLE II
ESTIMATED β AND α VALUES FOR THE DIFFERENT NODES (IN PARTS PER MILLION). β_n DENOTES THE VALUES OBTAINED WITH THE PROCEDURE DESCRIBED IN SECTION VI-B. $\alpha(\beta_n)$ IS OBTAINED FROM β_n VALUES USING (10), AND α_n VALUES ARE OBTAINED WITH THE PROCEDURE DESCRIBED IN SECTION IV. THE LAST ROW SHOWS THE DIFFERENCE BETWEEN THE TWO ESTIMATIONS

	NC	N1	N2	N3	N4	N5	N6
β_n	55.25	55.04	46.40	-9.67	48.39	54.48	47.97
$\alpha(\beta_n)$	–	-0.21	-8.85	-64.92	-6.86	-0.77	-7.28
α_n	–	0.11	-8.55	-64.93	-7.26	-0.44	-6.78
$\alpha_n - \alpha(\beta_n)$	–	0.32	0.30	-0.01	-0.40	0.33	0.50

The EUSART nominal clock frequency is fixed at $F_b = 80$ kHz, and the sampling frequency is fixed at $F_x = 500$ Hz. A reference square signal of frequency $F_m = 80125$ Hz is synthesized using a digital signal generator. The two square signals are mixed using a XOR gate, and the resulting signal is band limited at $F_x/2 = 250$ Hz and sampled with a digital oscilloscope. From a discrete Fourier transform (DFT) [31] analysis of the sampled signal, the frequency F_d of the maximum absolute value is then found, and the frequency shift is computed as $\Delta F_b = F_x/4 - F_d$. Finally, (37) is used to obtain the relative clock drift. A total number of 50 000 samples were acquired for each node EUSART clock, and a 625 000 point DFT was used to find the frequency F_d. The achieved frequency resolution is 0.8 mHz, which allows estimating the relative clock drift with a resolution of 0.01 ppm. Fig. 3 shows an example of the DFT of node N1 data showing a 4.4032-Hz frequency shift corresponding to a relative drift of 55.04 ppm. The measured drifts[4] for all nodes (including the coordinator) are shown in the first row (β_n) of Table II.

C. Clock Drift Effect Evaluation

Fig. 4 shows the effect of clock drifts in TOF measurements. Values are obtained using a pair of nodes, with N1 configured as transmitter and N6 as receiver. The distance between the nodes was approximately 3.5 m. The system was scheduled to perform

[4]The drift values are relative to the signal generator clock used as reference.

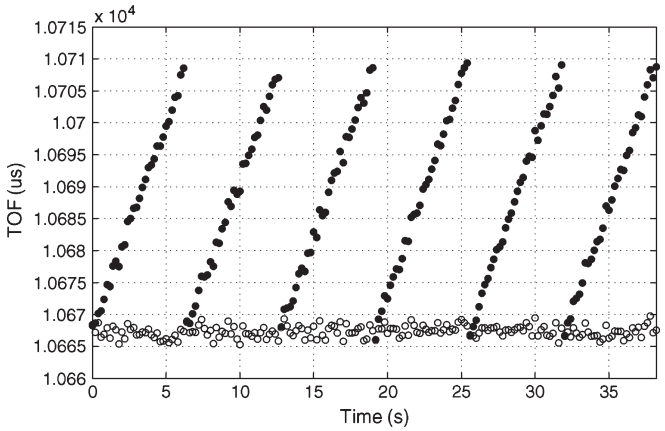

Fig. 4. TOF estimations using a couple of network nodes (N1 transmitter and N6 receiver) at an approximate distance of 3.5 m. The filled dots correspond to measures without clock drift compensation. The unfilled dots correspond to the same measures after correcting the bias due to the different clock drifts.

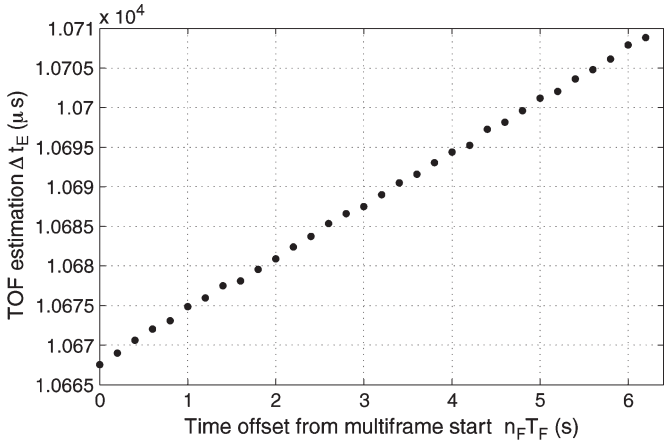

Fig. 5. Mean value of TOF estimations Δt_E versus the time offset from the multiframe start $n_F T_F$. Measurements obtained for a couple of nodes (N1 transmitter and N6 receiver) at an approximate distance of 3.5 m.

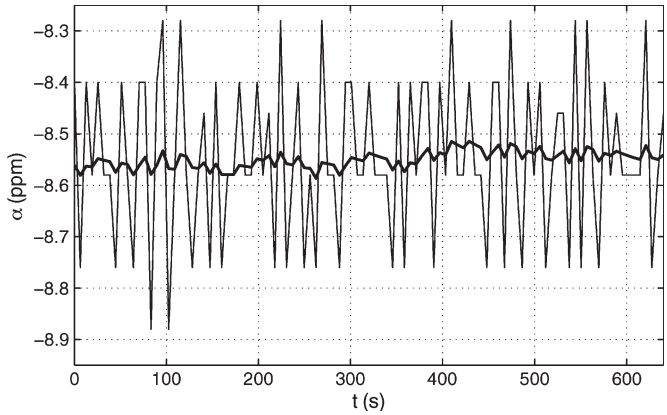

Fig. 6. Time evolution of the α estimation of node N2. The thin line corresponds to raw α estimations, while the thick line corresponds to the filtered version with $a = 0.1$.

32 measurements in each multiframe (one measurement every frame). The filled dots correspond to 192 TOF measurements (six multiframes) obtained without drift compensation.

In this case, the TOF error increases linearly with time and is reset at the beginning of every new multiframe. This is because a resynchronization occurs at the reception of a new synchronization message sent by the coordinator at the beginning of every multiframe. From Table II, the difference between the drifts of the transmitter (N1) and receiver (N6) nodes is $(\beta_T - \beta_R) = 7.07$ ppm. As predicted by (8), the maximum TOF error due to the different clock drifts occurs at the beginning of the last frame, which is 6.2 s from the beginning of the multiframe (considering 32 frames of 200 ms). The expected value of this error can be evaluated using (8) as $6.2 \times 7.07 \times 10^{-6} = 43.83$ μs, which explains the difference between maximum and minimum TOF values in the figure. The mean value of the data is 10 688.40 μs, and its standard deviation is 12.28 μs, which would correspond to 4.17 mm if the velocity of sound would be 340 m/s.

To obtain an estimation of the bias caused by the clock drifts of the nodes, the mean value of all measurements performed at the beginning of a given frame n_F of the multiframe is computed. The resulting values are plotted against the time offset from the beginning of the multiframe $n_F T_F$, as shown in Fig. 5, in which a clear dependence of the bias with this time offset is evident.

The linear model (8) is fitted to these data by minimum mean square error linear regression of the estimated TOF (identified with Δt_E) versus the time offset from the beginning of the multiframe $n_F T_F$. The obtained intercept is 10 667.85 μs, which corresponds to the average value of the compensated TOF. The obtained slope is 6.62×10^{-6}, which is identified with $\Delta\beta = (\beta_T - \beta_R)$ and very close to the 7.07-ppm theoretical value. From these values, a corrected TOF estimation can be obtained using (8) as $\widehat{\mathrm{TOF}} = \Delta t_E - n_F T_F \Delta\beta$. These values are plotted with unfilled dots in Fig. 4. Now, the linear trend is removed, and the mean value and standard deviation are 10 667.85 and 1.06 μs, respectively. These results show the correctness of the proposed linear model.

D. Estimation of α Values

To evaluate the clock drift estimation algorithm, α values from a set of 100 consecutive multiframes were recorded for each of the six end nodes (N1 to N6). The mean values for each node are shown in the third row of Table II. Comparison with the values obtained from the estimations of β (second row of the table) shows that the two methods provide consistent estimations with a difference of less than 0.5 ppm.

The time evolution of α estimations is shown in Fig. 6 for node N2. The thin line corresponds to raw values $a = 1.0$, while the thick line corresponds to filtered values with $a = 0.1$. The variance reduction due to the IIR filter is evident from this figure.

The standard deviations of $\hat{\alpha}_n$ for all six end nodes are shown in Table III for values of the IIR filter coefficient of $a = 1.0$, $a = 0.2$, and $a = 0.1$ for each node. The last column also shows the averaged values for all nodes in each case. These values are consistent with those predicted by the simulations. For the coordinator and node clock resolutions (second row of Table I), the simulations predict standard deviations of 0.1426, 0.0213, and 0.0104 ppm for IIR filter coefficient values of 1.0, 0.2, and 0.1, respectively; the corresponding measured values are (the last column of Table III) 0.144, 0.023, and 0.012. These results validate the proposed α estimation algorithm.

TABLE III
STANDARD DEVIATIONS OF α VALUES IN PARTS PER MILLION FOR THE DIFFERENT NODES AND FOR $a = 1.0$, $a = 0.2$, AND $a = 0.1$ VALUES OF THE IIR FILTER COEFFICIENT. THE VALUES FOR EACH NODE ARE OBTAINED FROM 100 α ESTIMATIONS FROM CONSECUTIVE MULTIFRAMES. THE LAST COLUMN (AVG) SHOWS THE AVERAGE VALUES CONSIDERING DATA FROM ALL SIX NODES IN EACH CASE

	N1	N2	N3	N4	N5	N6	Avg
$a = 1.0$	0.157	0.158	0.138	0.137	0.139	0.134	0.144
$a = 0.2$	0.025	0.026	0.022	0.022	0.024	0.021	0.023
$a = 0.1$	0.013	0.014	0.011	0.011	0.013	0.011	0.012

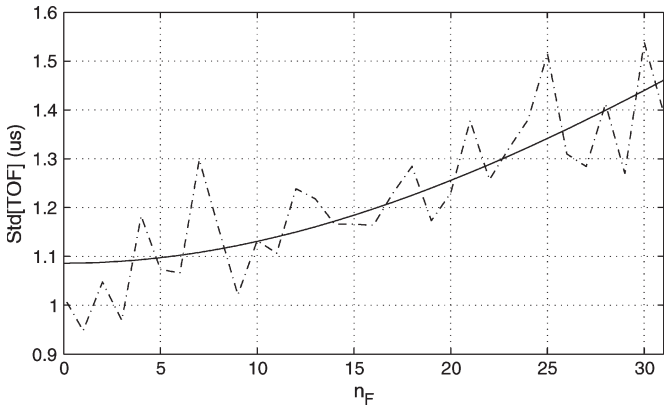

Fig. 7. TOF standard deviation as a function of the frame number. The discontinuous line is the standard deviation of TOF measurements in each frame n_F. The solid line is the result of fitting the model (35).

E. Effect of the Variance of α

Fig. 7 shows the variation of the TOF standard deviation with the frame number n_F. As discussed in Section IV, α variance contributes with a different weight to the total TOF variance depending on the frame number n_F. In this experiment, 8640 TOF measurements were recorded between a pair of nodes (N1 as transmitter and N6 as receiver) at an approximated distance of 2 m. The α estimation in the nodes was performed without IIR filtering, with coordinator clock resolution $T_c = 2$ μs and node clock resolution $T_o = 1$ μs. The system was scheduled to perform 32 TOF measurements per multiframe. A total of 270 TOF measurements is available for each frame of the multiframe. Each group of TOF measurements corresponding to the same frame index was used to estimate the corresponding variance. The theoretical relation (35) was fitted, and the resulting values are plotted with a solid line in the figure. The value $\sigma_\xi = 0.111$ μs obtained for the fitted curve is close to the theoretical value $\sigma_\xi = 0.1426$ μs (see Table III) and explains the different standard deviation of TOF measurements in each frame of the multiframe.

F. System Evaluation

In this section, we present an experimental evaluation of the whole system in terms of the achieved TOF accuracies. First, the same experimental study presented in Section VI-C is repeated for the pair of nodes N1 and N6 and using the same setup. Fig. 8 shows the estimated TOF after using the clock drift compensation algorithm described in Section III-A and the α estimation procedure described in Section IV with a value for the IIR filter coefficient $a = 0.1$. By comparing Figs. 8 and 4, it is evident that the clock drift effects have been removed. The

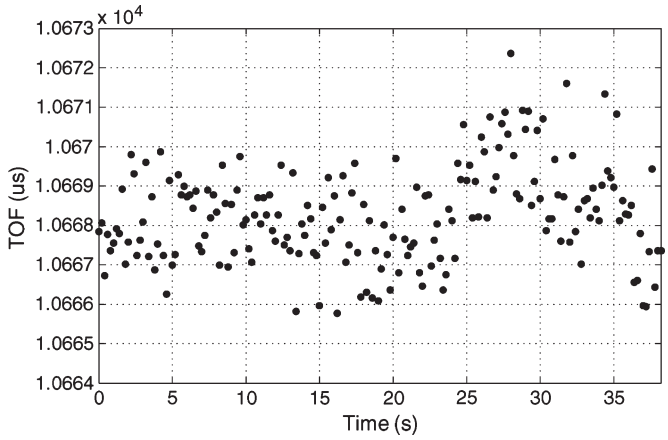

Fig. 8. TOF estimations using a couple of network nodes (N1 transmitter and N6 receiver) at an approximate distance of 3.5 m. Measurements have been obtained after using the clock drift compensation procedure described in Section III-A and the α estimation procedure described in Section IV with a value for the IIR filter coefficient $a = 0.1$.

TABLE IV
TOF STANDARD DEVIATIONS FOR FIVE PAIRS OF NODES AT THREE DIFFERENT DISTANCES FROM 1600 TOF MEASUREMENTS OF THE COMPLETE SYSTEM WITH CLOCK DRIFT COMPENSATION. α ESTIMATION IS PERFORMED WITH IIR FILTER COEFFICIENT $a = 0.1$. NODE N1 WAS CONFIGURED AS TRANSMITTER, AND NODES N2 TO N6 WERE CONFIGURED AS RECEIVERS. THE SYSTEM WAS SCHEDULED TO PERFORM 32 TOF MEASUREMENTS PER MULTIFRAME. THE LAST COLUMN SHOWS THE AVERAGED RESULTS FOR EACH DISTANCE ACROSS ALL NODE PAIRS

	TOF standard deviation (μs)					
Dist (mm)	N1-N2	N1-N3	N1-N4	N1-N5	N1-N6	Avg.
2000	0.67	0.95	1.01	0.96	0.95	0.92
3500	1.05	1.13	1.06	1.31	1.19	1.15
5500	1.70	2.13	1.89	1.87	1.82	1.89

mean value and standard deviation of the corrected TOF are now 10 668.19 and 1.27 μs, respectively. By repeating the same linear regression analysis previously presented in Section VI-C, the new slope and intercept values are 10 667.98 μs and 0.07 ppm, respectively, confirming that the clock drift effects have been effectively removed.

To evaluate the performance of the complete system, a set of TOF measurements was obtained from five different pairs of nodes at three different approximated distances of 2, 3.5, and 5.5 m. Node N1 was configured as transmitter, and nodes N2 to N6 as receivers. In all cases, α estimation was performed with an IIR filter coefficient $a = 0.1$ and with coordinator clock resolution $T_c = 2$ μs and node clock resolution of $T_o = 1$ μs. Clock drift compensation was also applied in all cases.

For each distance and node pair, a total of 1600 TOF measurements was recorded. Standard deviations are shown in Table IV for each node pair and distance along with the averaged values for each distance across all node pairs.

The TOF variance increases as a function of the distance, which is due to the SNR decrease of the ultrasonic signal that affects the σ_η term in (35). At a distance of 2 m, the averaged TOF standard deviation is 0.92 μs. Considering that the standard deviation contribution of the clock drift and resolution (see (35) and Section VI-D) is 0.58 μs, the contribution of σ_η can be approximately estimated as 0.71 μs. Increasing the distance yields to greater values of the TOF standard deviation. As the

contribution of the clock effects is independent of the distance, this greater TOF standard deviation is explained by an increase in the value of σ_η. The clock effects have less influence on the total TOF standard deviation value for greater distances, and therefore, in the current configuration, no significant improvement in the accuracy of the TOF estimation would be expected from improving the clock resolution.

Evaluation of the system performance in terms of standard deviation of the measured distance (for a typical sound speed value of 340 m/s) can be obtained from the standard deviation of TOF values in the last column of Table IV. For a distance of 2 m, the standard deviation of the distance will be 0.31 mm, while the corresponding values for 3.5 and 5.5 m are 0.39 and 0.64 mm, respectively. From these values, we can conclude that the system, in the absence of other error sources, is able to reach subcentimetric or even submillimetric precisions for distances below 6 m.

VII. Conclusion

In this paper, an ultrasonic TOF measurement system has been proposed in the context of wireless sensor networks. Restrictions due to the low-power, low-cost, and low-bit-rate conditions are considered in the design.

Generation and detection of ultrasonic signals are digitally performed with a reduced number of analog components and using low-cost ceramic ultrasonic transducers. TOF estimation is performed by the receptor nodes using a digital quadrature correlator based on a bandpass sampling scheme. Measurement synchronization is provided based on a TDMA scheduling approach.

Potential error sources due to the clock drifts of the microcontroller nodes are theoretically characterized, and techniques have been proposed to correct them. A theoretical error characterization of the whole measurement system is derived. The model takes into account both the drift and the finite clock resolution effects.

The measurement system has been implemented in a smart sensor network based on the ZigBee protocol. Experimental results supporting the theoretical derivations are shown. Even with clock resolutions on the order of 1 μs and clock drifts around 50 ppm, the system evaluation demonstrates the viability of obtaining subcentimetric distance precisions using inexpensive hardware.

The results of this paper are applicable to other ultrasonic distance measurement techniques within the proposed network-based measurement system.

However, the precision of the system depends not only on the node synchronization. There are several factors that can degrade the system precision in a real environment, such as multipath effect, air flows or variations in temperature, and relative humidity that may affect the speed of propagation of the ultrasonic signal. On the other hand, the use of passive components in the hardware design of the nodes introduces an additional delay in the TOF measurement. The estimation of such delay involves a calibration process of the nodes. Finally, the accuracy of the position of the mobile node also depends on a correct determination of the coordinates of the reference nodes. All these topics will be addressed in future works.

A frame duration of 200 ms allows performing a maximum of five TOF measurements per second. Considering a typical speed of the mobile node of 2 m/s, a displacement of 0.4 m will appear between consecutive measurements, leading to positioning errors. However, TELIAMADE system has a flexible configuration that allows using different strategies to address this problem.

The first strategy is to reduce the duration of frame to 50 ms, allowing a higher measurement rate and thus reducing the error due to displacement of the mobile node. However, a shorter frame period would reduce the available time for performing the position estimation and would require a faster microcontroller.

The second strategy is to reverse the operation way of nodes in TELIAMADE. The fixed nodes (typically located in the ceiling) can be configured as ultrasonic receivers, and the mobile node can be configured as an ultrasonic transmitter. So, the distance between the mobile and all the reference nodes can be estimated simultaneously, therefore avoiding possible errors due to the mobile node displacements. The main disadvantage of this configuration is that the privacy of the positioning is not guaranteed.

The third strategy is to use a synchronous CDMA scheme. By using pseudorandom codes, the fixed nodes can start simultaneously the signal transmission at the beginning of each frame. The orthogonality of these codes allows the receiver node to estimate the TOF of each individual signal. The location privacy is guaranteed since the mobile is responsible for estimating its position. On the other hand, the positioning rate is also increased and is conditioned by the selected frame period. Nevertheless, this strategy increases the computational load of the receiver node.

Selecting the most appropriate strategy will depend on the particular application.

References

[1] C. Falsi, D. Dardari, L. Mucchi, and M. Z. Win, "Time of arrival estimation for UWB localizers in realistic environments," *EURASIP J. Appl. Signal Process.*, vol. 2006, pp. 32 082-1–32 082-3, Jan. 2006.

[2] P. Bahl and V. Padmanabhan, "RADAR: An in-building RF-based user location and tracking system," in *Proc. IEEE Infocom*, Los Alamitos, CA, 2000, pp. 775–784.

[3] T. A. Alhmiedat and S.-H. Yang, "A ZigBee-based mobile tracking system through wireless sensor networks," *Int. J. Adv. Mechatron. Syst.*, vol. 1, no. 1, pp. 63–70, 2008.

[4] L. M. Ni, Y. Liu, Y. C. Lau, and A. P. Patil, "Landmark: Indoor location sensing using active RFID," *Wireless Networks. Special Issue on Pervasive Computing and Communications*, vol. 10, no. 6, pp. 701–710, 2004.

[5] J. Krumm, S. Harris, B. Meyers, B. Brumitt, M. Hale, and S. Shafer, "Multi-camera multiperson tracking for easy living," in *Proc. 3rd IEEE Int. Workshop Visual Surveillance*, Dublin, Ireland, Jul. 2000, pp. 3–10.

[6] A. Harter, A. Hopper, P. Steggles, A. Ward, and P. Webster, "The anatomy of a context-aware application," in *Proc. 5th Annu. ACM/IEEE Int. Conf. Mobicom*, 1999, pp. 59–68.

[7] N. B. Priyantha, A. Chakraborty, and H. Balakrishnan, "The CRICKET location-support system," in *Proc. 6th ACM MOBICOM*, 2000, pp. 32–43.

[8] M. Hazas and A. Hopper, "Broadband ultrasonic location systems for improved indoor positioning," *IEEE Trans. Mobile Comput.*, vol. 5, no. 5, pp. 536–547, May 2006.

[9] J. C. Prieto, A. R. Jiménez, J. I. Guevara, J. L. Ealo, F. A. Seco, J. O. Roa, and F. Ramos, "Performance evaluation of 3D-LOCUS advanced acoustic LPS," *IEEE Trans. Instrum. Meas.*, vol. 58, no. 8, pp. 2385–2395, Aug. 2009.

[10] J. C. Prieto, A. R. Jiménez, J. I. Guevara, J. L. Ealo, F. A. Seco, J. O. Roa, and F. Ramos, "Subcentimeter-accuracy location through broad-band acoustic transducers," in *Proc. IEEE Int. Symp. Intell. Signal Process.*, Oct. 3–5, 2007, pp. 929–934.
[11] A. Marco, R. Casas, J. Falco, H. Gracia, and J. A. A. Roy, "Location-based services for elderly and disabled people," *Comput. Commun.*, vol. 31, no. 6, pp. 1055–1066, Apr. 2008.
[12] S.-B. Jiang, C.-M. Yang, R.-S. Huang, C.-Y. Fang, and T.-L. Yeh, "An innovative ultrasonic time-of-flight measurement method using peak time sequences of different frequencies: Part I," *IEEE Trans. Instrum. Meas.*, vol. 60, no. 3, pp. 735–744, Mar. 2011.
[13] W. M. Waters and B. R. Harret, "Bandpass signal sampling and coherent detection," *IEEE Trans. Aerosp. Electron. Syst.*, vol. AES-18, no. 6, pp. 731–736, Nov. 1982.
[14] J. L. Brown, Jr., "On quadrature sampling of bandpass signals," *IEEE Trans. Aerosp. Electron. Syst.*, vol. AES-15, no. 3, pp. 366–371, May 1979.
[15] C. Medina, J. C. Segura, and A. de la Torre, "TELIAMADE: Sistema de localización en interiores basado en ultrasonido y RF," in *Proc. 25th Simp. Nacional URSI*, Sep. 2010, p. 39.
[16] C. Medina, J. C. Segura, and A. de la Torre, "Una red inalámbrica de sensores orientada a localización con precisión subcentimétrica," in *Proc. 26th Simp. Nacional URSI*, Sep. 2011, pp. 5–8.
[17] *Zigbee Protocol Specification*, ZigBee Alliance Inc., San Ramon, CA, 2007.
[18] B. Sundararaman, U. Buy, and A. D. Kshemkalyani, "Clock synchronization for wireless sensor network: A survey," *Ad Hoc Netw.*, vol. 3, no. 3, pp. 281–323, 2005.
[19] J. Elson, L. Girod, and D. Estrin, "Fine-grained network time synchronization using reference broadcast," in *Proc. 5th 19th Symp. OSDI*, 2002, vol. 36, pp. 147–163.
[20] M. Mock, R. Frings, E. Nett, and S. Trikaliotis, "Continuous clock synchronization in wireless real-time applications," in *Proc. 19th IEEE SRDS*, Oct. 2000, pp. 125–133.
[21] J.-P. Sheu, W.-K. Hu, and J.-C. Lin, "Ratio-based time synchronization protocol in wireless sensor networks," *Telecommun. Syst.*, vol. 39, no. 1, pp. 25–35, Sep. 2008.
[22] O. Mirabella, M. Brischetto, A. Raucea, and P. Sindoni, "Dynamic continuous clock synchronization for IEEE 802.15.4 based sensor networks," in *Proc. IEEE IECON*, Orlando, FL, 2008, pp. 2438–2444.
[23] *28/40/44-Pin Enhanced Flash Microcontrollers With 10-Bit A/D and NanoWatt Technology*, PIC18F2525/2620/4525/4620, 2008.
[24] *CC2420 2.4 GHz IEEE 802.15.4/ZigBee-Ready RF Transceiver*, Texas Instruments, Dallas, TX.
[25] *Air Ultrasonic Ceramic Transducers*, 400ST/R120.
[26] *74HC04, 74HCT04 Hex Inverter Datasheet*, NXP Semicond., Eindhoven, The Netherlands, 2012.
[27] *LMC6482CMOS Dual Rail-To-Rail Input and Output Operational Amplifier*, Nat. Semicond., Santa Clara, CA, 2003.
[28] D. Marioli, C. Narduzzi, C. Offelli, D. Petri, E. Sardini, and A. Taroni, "Digital time-of-flight measurement for ultrasonic sensors," *IEEE Trans. Instrumentation and Measurement*, vol. 41, no. 1, pp. 93–97, Feb. 1992.
[29] F. Halsall, *Multimedia Communications. Applications, Networks, Protocols ans Standards*. Upper Saddle River, NJ: Pearson Educ., 2001, ch. 11, pp. 722–730.
[30] B. Lathi and Z. Ding, *Modern Digital and Analog Communication Systems*. Oxford, U.K.: Oxford Univ. Press, 2009, ser. Electrical and Computer Engineering.
[31] A. Oppenheim and R. Schafer, *Discrete-Time Signal Processing*. Englewood Cliffs, NJ: Prentice-Hall, 1989.

Carlos Medina received the B.S. degree in telecommunications engineering and the M.S. degree in multimedia systems from the University of Granada (UGR), Granada, Spain, where he is currently working toward the Ph.D. degree in the Department of Signal Theory, Telematics and Communications (TSTC). He was granted a Ph.D. fellowship by the Andalusian Regional Government on September 2009.

His research interests include wireless sensor networks and indoor positioning systems based on ultrasound and radio frequency.

José C. Segura (M'93–SM'03) received the M.S. degree in physics and the Ph.D. degree in variants of Hidden Markov Model modeling for speech from the University of Granada (UGR), Granada, Spain, in 1984 and 1991, respectively.

He was an Assistant Professor of electronics with the Department of Electronics and Computer Technology, UGR, and the Vice Director of the Centre for Information Services and Communications, UGR. He is currently a Full Professor of signal theory and communications with the Department of Signal Theory, Telematics and Communications (TSTC), UGR, where he is the Vice Director of the Information and Communications Technology Research Centre (CITIC). He is a Reviewer for several scientific journals. His current research interests include ultrasonic signal processing, sensor networks, signal processing, communication systems, and speech recognition.

Ángel de la Torre received the M.Sc. and Ph.D. degrees in physics from the University of Granada (UGR), Granada, Spain, in 1994 and 1999, respectively.

Since 1994, he has been with the Research Group on Signals, Telematics and Communications, Department of Signal Theory, Telematics and Communications (TSTC), UGR, where he is an Associate Professor since 2003. In 2000, he joined the PAROLE Group, Laboratoire Reconnaissance des Formes et Intelligence Artificielle, Laboratoire Lorrain de Recherche en Informatique et ses Aplications, Nancy, France, as a Postdoctoral Researcher in the field of robust speech recognition and the Institut für Angewandte Physik, Innsbruck, Austria, as a Postdoctoral Researcher in the field of cochlear implants. He is a Reviewer for several scientific journals. His research interests are in the field of signal processing and particularly robust speech recognition, speech processing in noise conditions, signal processing for cochlear implants, processing of seismic signals, acquisition and processing of electrophysiological responses in audiology, and processing of mass spectrometry data.